Chapter 6

Observation and Investigation of Increasing Isosteric Heat of Adsorption of Ethane on Zeolite-Templated Carbon

M. Murialdo, N.P. Stadie, C.C. Ahn, and B. Fultz, "Observation and Investigation of Increasing Isosteric Heat of Adsorption of Ethane on Zeolite-Templated Carbon," J. Phys. Chem. C, 119, 994 (2015).
DOI: 10.1021/jp510991y
http://pubs.acs.org/doi/abs/10.1021/jp510991y

Abstract

Ethane adsorption was measured on zeolite-templated carbon (ZTC) and compared to superactivated carbon MSC-30. Isotherms measured at temperatures between 252 and 423 K were fitted using a superposition of two Langmuir isotherms and thermodynamic properties were assessed. Unlike typical carbon adsorbents, the isosteric heat of adsorption on ZTC increases by up to 4.6 kJ mol^{-1} with surface coverage. This increase is attributed to strong adsorbate-adsorbate intermolecular interactions, a hypothesis that is shown to be consistent with fundamental estimates of intermolecular interactions. Furthermore, the molar entropy of the adsorbed phase was measured and compared to an estimate derived from statistical mechanics. While the measured and estimated entropies of the adsorbed phase of ethane on MSC-30 are in agreement, they differ significantly on ZTC at high coverage, indicative of the atypical properties of ethane adsorption on ZTC.

1. Introduction

Ethane is the second most abundant component in natural gas and an important petrochemical feedstock. It is a common reactant for the synthesis of ethylene, and its separation from natural gas has been an important process for many years. Currently, the separation of ethane from natural gas is predominantly carried out via cryogenic distillation, an energy intensive process.[1] Physisorption materials have been proposed as a more efficient separation solution.[2,3,4] Physisorption materials also hold promise in improving the volumetric energy density of stored ethane.[5,6] An understanding of ethane adsorption is thus essential for natural gas storage and separation processes.

Physisorption occurs when weak physical interactions between a solid adsorbent and a gas induce the formation of a locally densified adsorbate layer at the solid surface. This interaction depends sensitively on the surface chemistry and surface structure of the adsorbent.[7,8,9,10] The isosteric heat of adsorption, q_{st}, is often reported as a critical figure of merit for physisorption. This proxy measure of binding energy determines the equilibrium uptake quantity at finite temperatures and pressures.

Microporous carbons have gained significant attention as potential adsorbents due their light weight, low cost, and wide variability.[11,12,13] However, these materials often exhibit binding energies that are below desired optimal values.[14,15] Furthermore, the isosteric heat of adsorption typically decreases with surface coverage due to binding site heterogeneity, further reducing the deliverable gas storage capacity in the range of practicality for applications. We recently reported the observation of increasing isosteric heat of adsorption of methane on zeolite-templated carbon,[16] a unique and anomalous behavior with respect to methane which typically has very weak intermolecular interactions. Recently, Yuan et al. reported the synthesis

of a mesoporous carbon wherein the isosteric heat of ethane adsorption increases as a function of coverage.[17] This was attributed to favorable ethane-ethane intermolecular interactions and a relatively homogeneous adsorbent surface. While intriguing, the latter results have limited applications for gas storage and separation due to limitations of the mesoporous carbon in question. With an average pore width of 48 Å and a specific surface area of 599 m^2 g^{-1}, this mesoporous carbon has only a small total excess uptake capacity of ~2.5 mmol g^{-1} at 278 K. This effect has not been investigated or observed for ethane adsorption on a *microporous* carbon with a large specific surface area, a system that would have superior potential for advanced applications. In this work, we report that a zeolite-templated carbon (ZTC) with a narrow distribution of pore widths centered at 12 Å and a large specific surface area of 3591 m^2 g^{-1} exhibits an increasing isosteric heat of ethane adsorption as a function of coverage. This material has an exceptional uptake capacity of 22.8 mmol g^{-1} (at 252K), owing to its very large surface area and optimized structural properties. Furthermore, several novel analysis methods including comparisons to methane adsorption, Lennard-Jones parameters and statistical mechanics calculations are implemented to corroborate and assist in the understanding of the phenomenon of increasing isosteric heat of adsorption.

2. Experimental Methods

2.1 Materials Synthesis

Two materials were chosen for comparison in this study: MSC-30 and ZTC. The superactivated carbon "Maxsorb" MSC-30 was obtained from Kansai Coke & Chemicals Company Ltd. (Japan). The zeolite-templated carbon (ZTC) was synthesized in a multistep process that was optimized to achieve high template fidelity of the product.[18] The faujasite-

type zeolite NaY (obtained from Tosoh Corp., Japan) was impregnated with furfuryl alcohol which was subsequently polymerized at 150 °C, augmented by a propylene CVD step at 700 °C, and carbonized at 900 °C. The ZTC product was freed by dissolution of the zeolite template in HF. ZTC was confirmed to exhibit very high fidelity with the zeolite template and outstanding microporous periodicity by X-ray diffraction and transmission electron microscopy, described in detail elsewhere.[16]

2.2 Materials Characterization

Equilibrium nitrogen adsorption isotherms were measured at 77 K using a BELSORP-max volumetric instrument from BEL-Japan Inc. The Dubinin-Radushkevich (DR) method[19,20] was employed to calculate micropore volumes and the Brunauer-Emmett-Teller (BET) method[21] was used to calculate specific surface areas. Pore-size distributions were determined by non-local density functional theory (NLDFT) analysis implemented by software provided by Micromeritics Instrument Corp., and a carbon slit-pore model was utilized.[22] Skeletal densities of the materials were determined by helium pycnometry. Finally, the Dumas method[23] was employed to determine the elemental composition (CHN) of MSC-30 and ZTC.[24]

2.3 Measurements

Equilibrium ethane adsorption isotherms were measured on ZTC and MSC-30 at 9 temperatures between 252 and 423 K. Research grade ethane (99.999%) obtained from Matheson Tri-Gas Inc. was used in a custom Sieverts apparatus that was tested for accuracy up to 10 MPa.[25] The reactor containing the sample was held at a constant set temperature while the remaining gas manifold always remained at room temperature. For low temperature isotherms, the reactor was submerged in a circulated chiller bath leading to temperature

deviations no larger than $\pm$0.1 K. For high temperature isotherms, the reactor was encased in a copper heat exchanger and wrapped with insulating fiberglass-heating tape. A PID controller was used to maintain a constant temperature with fluctuations of less than $\pm$0.4 K. In both setups, the temperature was measured by K-type thermocouples placed in direct contact with the reactor. The manifold temperature was measured with a platinum resistance thermometer in contact with the outer wall of the manifold.

High-pressure measurements were made with an MKS Baratron (Model 833) pressure transducer. For degassing, vacuum pressures were ensured with a digital cold cathode pressure sensor (I-MAG, Series 423). The Sieverts apparatus is equipped with a molecular drag pump capable of achieving vacuum of 10^{-4} Pa. Each sample was degassed at 520 K under vacuum of less than 10^{-3} Pa prior to measurements. Multiple adsorption/desorption isotherms were measured to ensure reversibility, and errors between identical runs were less than 1%. Gas densities were determined using the REFPROP Standard Reference Database.[26]

3. Results

3.1 Adsorbent Characterization

BET specific surface areas of ZTC and MSC-30 were found to be 3591 $\pm$ 60 and 3244 $\pm$ 28 $m^2\ g^{-1}$, respectively. Likewise, both materials have similar DR micropore volumes: 1.66 mL g^{-1} (ZTC) and 1.54 mL g^{-1} (MSC-30). The distribution of the pore sizes, however, differs significantly between the two materials. ZTC was determined to have a uniform pore-size distribution centered at 12 Å (see Figure 1). Over 90% of the micropore volume of ZTC is contained in pores with widths between 8.5 and 20 Angstroms. MSC-30 exhibits a wide range of pore sizes from 6 to 35 Å. 40% of the pore volume of MSC-30 is contained in pore widths

greater than 21 Angstroms. Furthermore, while MSC-30, like most activated carbons, has a skeletal density of 2.1 g mL^{-1}, ZTC has an unusually low skeletal density of 1.8 g mL^{-1} (in agreement with other ZTCs).[24] This discrepancy can be explained by the significantly higher hydrogen content found in ZTC by elemental analysis experiments. Hydrogen was found to account for 2.4% (by weight) of ZTC but only 1.2% of MSC-30.[24]

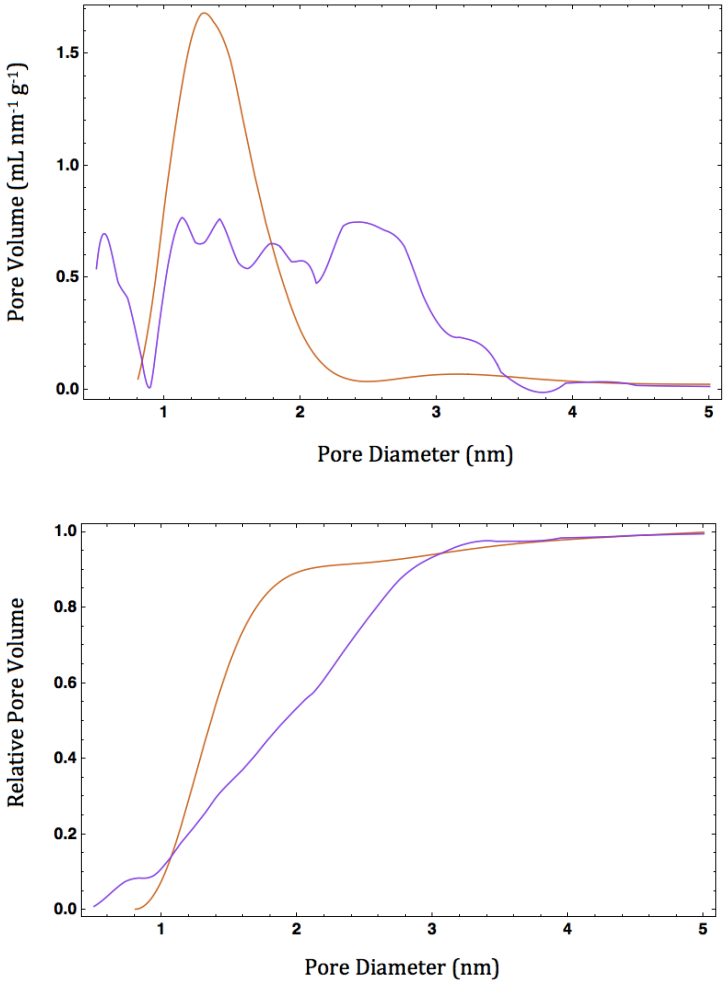

Figure 1. Pore-size distribution and relative pore volume of ZTC (orange) and MSC-30 (purple).

3.2 Adsorption Measurements:

Equilibrium ethane adsorption isotherms were measured at 9 temperatures between 252 and 423K and at pressures of up to 32 bar (see Figure 2). The maximum excess adsorption quantities measured on ZTC and MSC-30 (at ~253K) were 22.8 and 26.8 mmol g^{-1}, respectively. At room temperature (297K), the maximum uptake quantities measured on ZTC and MSC-30 were 19.2 and 22.1 mmol g^{-1}, respectively. Thus at both temperatures, MSC-30 exhibits greater excess adsorption capacities, with differences between the maximums being less than 15%. This is in contrast to methane adsorption on the same two materials, where ZTC exhibited higher excess adsorption capacities than MSC-30 at low temperatures.[16] Moreover, the differences in excess adsorption capacities between the two materials are smaller (less than 5%) for methane adsorption.

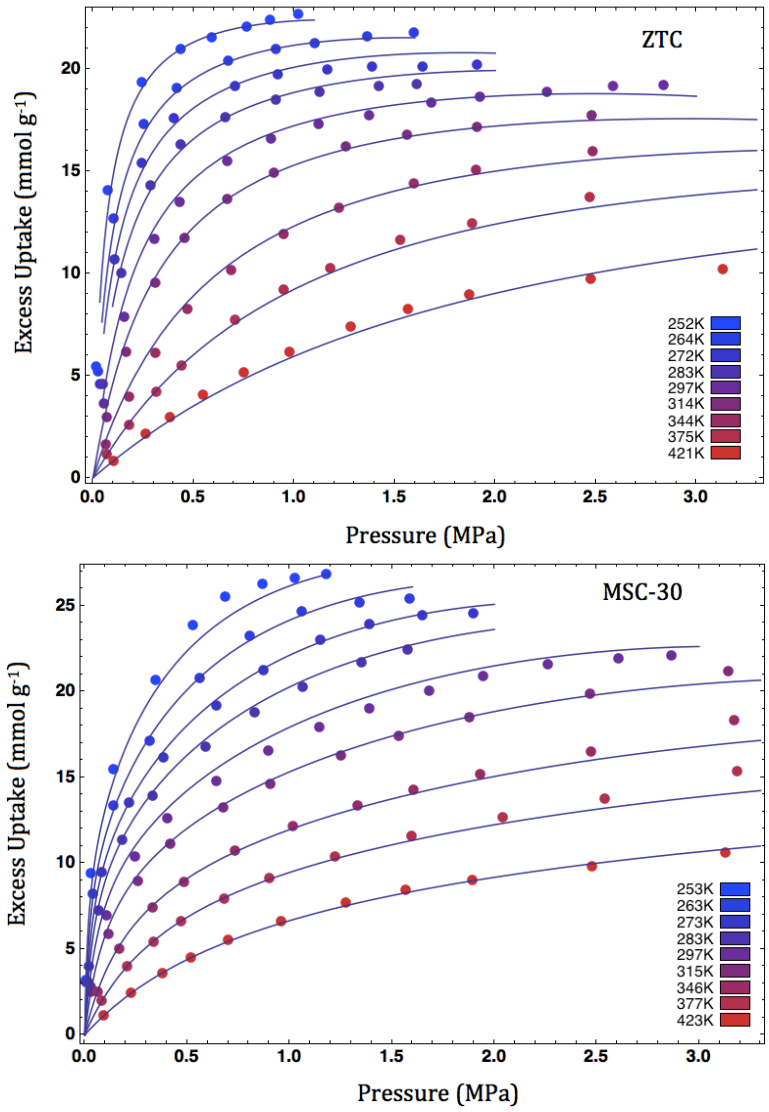

Figure 2. Equilibrium excess adsorption isotherms of ethane on ZTC and MSC-30. The lines indicate the best-fit analysis using a superposition of two Langmuir isotherms.

4. Discussion

4.1 Fitting Methodology

Thermodynamic analysis of adsorption requires interpolation of the adsorption data points, generally with a fitting function. It is common in literature to assume that the excess

adsorption well approximates the absolute adsorption. This assumption, while valid at low pressures and high temperatures, is invalid at temperatures near the critical point, particularly in high-pressure studies. To determine the absolute adsorption quantities and avoid the well-documented errors associated with equating excess adsorption and absolute adsorption, we follow a method initially described by Mertens.[27] We extend this method by modifications for the nonideal gas regime.[16]

The Gibbs excess adsorption[28] (n_e) is a function of the bulk gas density (ρ):

$$n_e = n_a - V_a\rho \quad (1)$$

Determining the absolute adsorption quantity (n_a) is simplest when the volume of the adsorption layer (V_a) is known. We left V_a as an independent fitting parameter, and assessed it later. The measured excess adsorption quantities were fitted with a generalized (multi-site) Langmuir isotherm:

$$n_e(P,T) = (n_{max} - V_{max}\rho(P,T))\left[\sum_i \alpha_i \frac{K_i P}{1+K_i P}\right] \quad (2)$$

Excess adsorption and density are functions of pressure (P) and temperature (T). The independent fitting parameters in this fitting model are n_{max}, a scaling factor indicative of the maximum absolute adsorption, α_i, a weighting factor for the i^{th} Langmuir isotherm($\sum_i a_i = 1$), V_a, which scales with coverage up to V_{max} (the maximum volume of the adsorption layer), and K_i, an equilibrium constant for the i^{th} Langmuir isotherm. The parameter K_i is defined by an Arrhenius-type equation:

$$K_i = \frac{A_i}{\sqrt{T}} e^{-E_i/RT} \quad (3)$$

Here, A_i is a prefactor and E_i is a binding energy associated with the i^{th} Langmuir isotherm. Using two superimposed isotherms (i=2), we obtained satisfactory results while limiting the number of independent fitting parameters to 7: n_{max}, V_{max}, α_1, A_1, A_2, E_1, and E_2. For ZTC and MSC-30, accurate fits were obtained with residual mean square values of 0.21 and 0.13 (mmol g^{-1})^2. These fits are shown in Figure 2 and the best-fit values of the fitting parameters are given in Table 1. For comparison, fitting parameters for methane adsorption on ZTC and MSC-30 were obtained using the same fitting procedure[16], and are also shown in Table 1.

Table 1. Least-squares minimized fitting parameters of the excess adsorption isotherms of ethane on MSC-30 and ZTC described by a two-site Langmuir isotherm.

	n_{max}	V_{max}	α_1	A_1	A_2	E_1	E_2
Ethane on ZTC	25 mmol/g	1.6 mL/g	0.82	2.1E-7 $K^{1/2}$/MPa	0.044 $K^{1/2}$/MPa	41 kJ/mol	18 kJ/mol
Ethane on MSC-30	36 mmol/g	2.6 mL/g	0.71	0.086 $K^{1/2}$/MPa	0.0065 $K^{1/2}$/MPa	20 kJ/mol	18 kJ/mol
Methane on ZTC	36 mmol/g	2.0 mL/g	0.46	0.059 $K^{1/2}$/MPa	0.00018 $K^{1/2}$/MPa	12 kJ/mol	20 kJ/mol
Methane on MSC-30	41 mmol/g	2.3 mL/g	0.70	0.068 $K^{1/2}$/MPa	0.0046 $K^{1/2}$/MPa	13 kJ/mol	13 kJ/mol

Many of the independent fitting parameters in this method have physical significance. For example, n_{max} represents the maximum specific absolute adsorption of the system. If the entire micropore volume of the material is assumed to be completely filled at this condition, then it follows that it should be approximately comparable to the value obtained by multiplying the density of the liquid phase of the adsorbate by the total micropore volume.

Using the density of liquid ethane and liquid methane near the triple point,[26] the maximum possible adsorption quantities estimated in this simplified way for ethane and methane on MSC-30 are 33 and 43 mmol g^{-1}, respectively. These values are within 10% of the n_{max} values determined through fitting. For ethane and methane adsorption on ZTC, the estimated and fitted values of n_{max} both deviate more significantly, with estimated values greater by 44% and 32% respectively.

The V_{max} parameter approximates the maximum volume of the adsorbed layer. Dividing by surface area, this gives an average width for the adsorbed layer. For ethane and methane adsorption on ZTC, this gives average adsorbed layer widths of 4.5 and 5.5 Å, both of which are in agreement with the measured ZTC micropore half-width of 6 Å. This suggests fairly effective filling of the ZTC micropores. Likewise, the ethane and methane V_{max} parameters on MSC-30 give adsorbed layer widths of 8 and 7 Å, which are in agreement with the average measured micropore half-width, 7 Å. Furthermore, for ethane on ZTC, V_{max} equals 1.6 mL g^{-1}, which is in good agreement with the micropore volume measured using the DR method and nitrogen isotherms, 1.66 mL g^{-1}. The V_{max} values for ethane on MSC-30 and methane on both materials deviate more significantly from measured DR micropore volumes with discrepancies of up to 41%. This, however, is not unexpected as different adsorbates with differing size and shape are confined and adsorbed in micropores distinctly.

4.2 Isosteric Enthalpy of Adsorption

The isosteric enthalpy of adsorption (ΔH_{ads}) is a widely used figure of merit that is indicative of the strength of binding interactions at a fixed temperature, pressure, and coverage. Typically it is determined using the isosteric method and reported as a positive value,

q_{st}, the so-called isosteric heat (a convention that is followed herein), defined according to the Clapeyron equation:

$$q_{st} = -\Delta H_{ads} = -T\left(\frac{\partial P}{\partial T}\right)_{n_a}(\Delta v_{ads}) \quad (4)$$

The molar change in volume of the adsorbate upon adsorption (Δv_{ads}) is given by the difference between the gas-phase molar volume and $\frac{V_{max}}{n_{max}}$. The fitting method used in this work is especially convenient for thermodynamic calculations with the Clapeyron equation because the generalized Langmuir equation with i=2 can be analytically differentiated.[27] The isosteric heats of adsorption of ethane on ZTC and MSC-30 calculated in this way are shown in Figure 3.

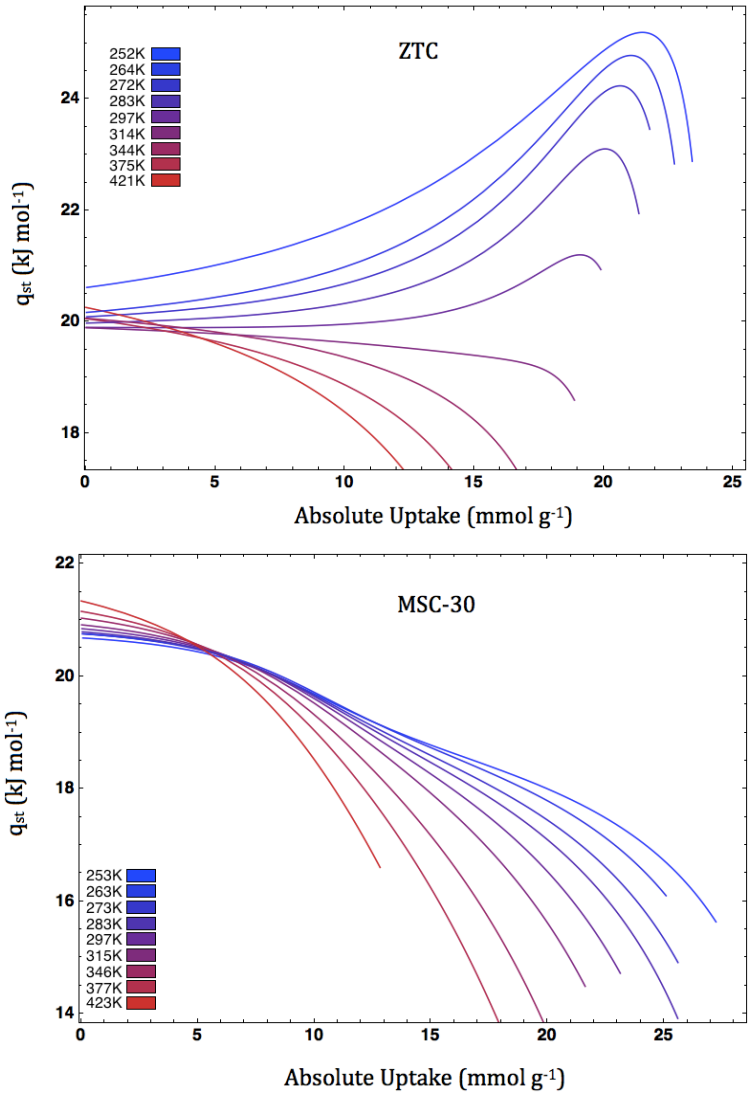

Figure 3. Isosteric heats of ethane adsorption on ZTC and MSC-30.

It can be observed that the isosteric heat of adsorption of ethane on ZTC increases as a function of coverage while MSC-30 (and a majority of other known systems) exhibits the typical decreasing isosteric heat with coverage (in this case represented as the absolute uptake quantity). This effect is most pronounced at low temperatures where the isosteric heat rises by 4.6 kJ mol^{-1} above its Henry's Law value of 20.6 kJ mol^{-1} (at 252 K). This effect (an increasing isosteric heat of adsorption) has also been observed for methane adsorption on the same material (ZTC)[16] and is dependent on gas properties as well as structural and surface properties

of the adsorbent. In particular, the effect is expected to increase with the strength of intermolecular interactions of the adsorbate when adsorbate molecules are on nanostructured surfaces that promote intermolecular interactions. ZTC is an ideal candidate adsorbent for observing such a phenomenon due to its uniform pore-size distribution with pore widths centered at 12 Å and homogeneous chemical nature[24].

In the absence of intermolecular interactions and binding site heterogeneity, the isosteric heat should be constant at all coverages and temperatures. The increase in isosteric heat (as a function of coverage) reported in this work is hypothesized to result from attractive intermolecular interactions between ethane molecules. Assuming random site occupancy in the low coverage regime (e.g. less than 50% of the available sites filled), the probability of any site being occupied is equal to the fractional site occupancy, θ. If z is the number of nearest neighbor adsorption sites, on average an adsorbate molecule will have $z\theta$ occupied nearest neighbor adsorption sites. By assuming that nearest neighbor interactions have a binding energy of ε and higher order neighbors have a negligible binding energy, the average adsorbate-adsorbate binding energy per molecule, ξ, is given:

$$\xi = \frac{z\theta\varepsilon}{2} \qquad (5)$$

Taking the derivative of ξ with respect to θ gives the estimated slope of the isosteric heat as a function of coverage (resulting from adsorbate-adsorbate interactions):

$$\frac{\partial(\xi)}{\partial\theta} = \frac{z\varepsilon}{2} \qquad (6)$$

The Lennard-Jones parameter ε (which describes the well depth of the Lennard-Jones 12-6 interaction potential) is 1.7 kJ mol^{-1} for ethane-ethane interactions[29]. For adsorbed molecules on a two-dimensional surface the number of nearest neighbor adsorption sites, z, is posited to

be 4. This results in an estimated slope for ethane on ZTC of 3.4 kJ mol^{-1}. The average slope of the measured isosteric heat of adsorption of ethane on ZTC (Figure 3) has a similar value of 3.3 kJ mol^{-1} (at the lowest measured temperature 252K, up to 50% coverage). Interestingly, these measured and estimated slopes are of a similar magnitude to the slope of the isosteric heat of ethane adsorption on the mesoporous carbon of Yuan et al. (~4-5 kJ mol^{-1} at ~298K).[17]

This very simple model (Equation 6) also gives a reasonable estimate for the increase in the isosteric heat of methane adsorption on ZTC. Here, ε for methane-methane interactions is 1.2 kJ mol^{-1},[29] giving a predicted slope of 2.4 kJ mol^{-1}. This is in agreement with the measured slope of 2.2 kJ mol^{-1} (up to 50% coverage at 255K).[16] It is important to note that z=4, while intuitively reasonable, is a posited value. The true value of z is difficult, if not impossible, to obtain, and likely varies for different gases.

A number of metrics suggest that ethane has stronger attractive intermolecular interactions than methane by a factor of ~1.4 to 1.6. These metrics include Lennard-Jones potential (adsorbate-adsorbate) well depth, boiling point, and critical temperature, and are shown in Table 2.

Table 2. Gas properties of ethane and methane and their ratios.

	ethane	methane	ratio
ε (Lennard-Jones)	1.7 kJ/mol[29]	1.2 kJ/mol[29]	1.4
Boiling Point (1 atm)	184.57 K[26]	111.67 K[26]	1.6528
Critical Temperature	305.32 K[26]	190.56 K[26]	1.6022

In agreement with the ratios in Table 2, the ratio of the slopes of the ethane and methane heats of adsorption (as a function of coverage) on ZTC is 1.5. Stronger

intermolecular interactions within ethane correspond to an isosteric heat that increases more steeply than methane on the same material. Furthermore, the average Henry's Law values (zero coverage limit) of the isosteric heat were determined to be 20 and 21 kJ mol^{-1} for ethane on ZTC and MSC-30, respectively, and 14 and 15 kJ mol^{-1} for methane. For both ZTC and MSC-30, these ratios of Henry's law values are 1.4 for ethane and methane.

4.3 Entropy

At equilibrium, the Gibbs free energy of the adsorbed phase (G_a) equals the Gibbs free energy of the gas phase (G_g). The isosteric entropy of adsorption (ΔS_{ads}) is

$$\Delta G_{ads} = Ga - Gg = \Delta H_{ads} - T\Delta S_{ads} = 0 \quad (7)$$

$$\Delta S_{ads} = \frac{\Delta H_{ads}}{T} \quad (8)$$

The isosteric entropy of adsorption is the change in entropy of the adsorbate upon adsorption and the measured values for ethane adsorption on MSC-30 and ZTC are shown in Figure 4 (reported as positive values).

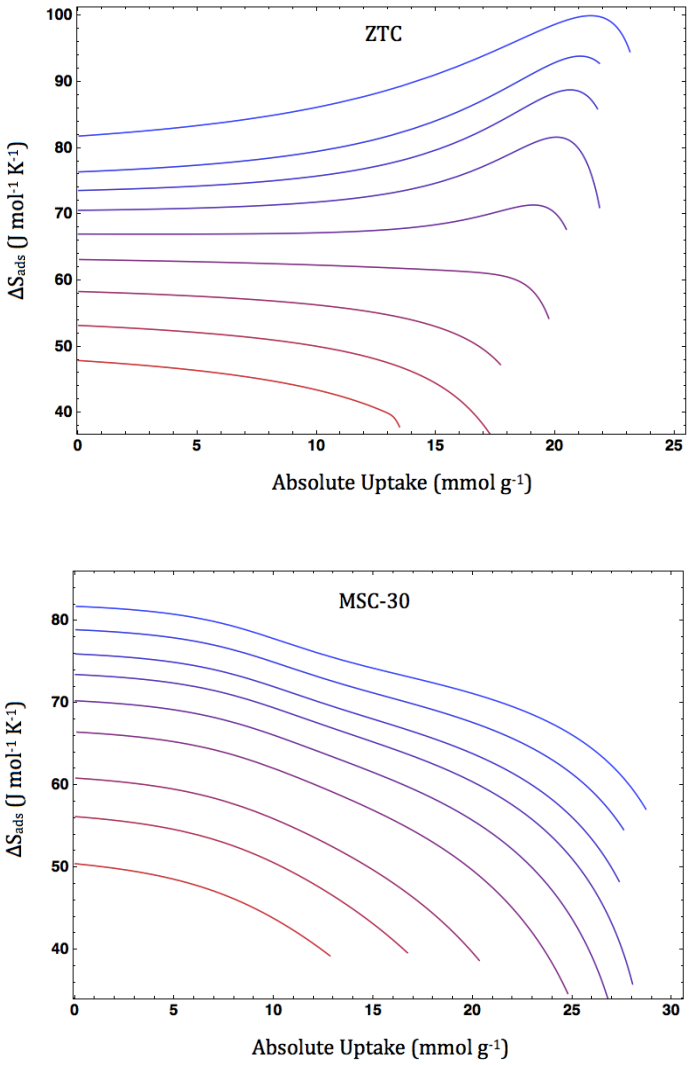

Figure 4. The isosteric entropy of ethane adsorption on ZTC and MSC-30 between 252 and 423 K.

By adding the isosteric entropy of adsorption to the gas-phase entropy (from Refprop[26]) we obtain the molar entropy of the adsorbed phase (Figure 5).

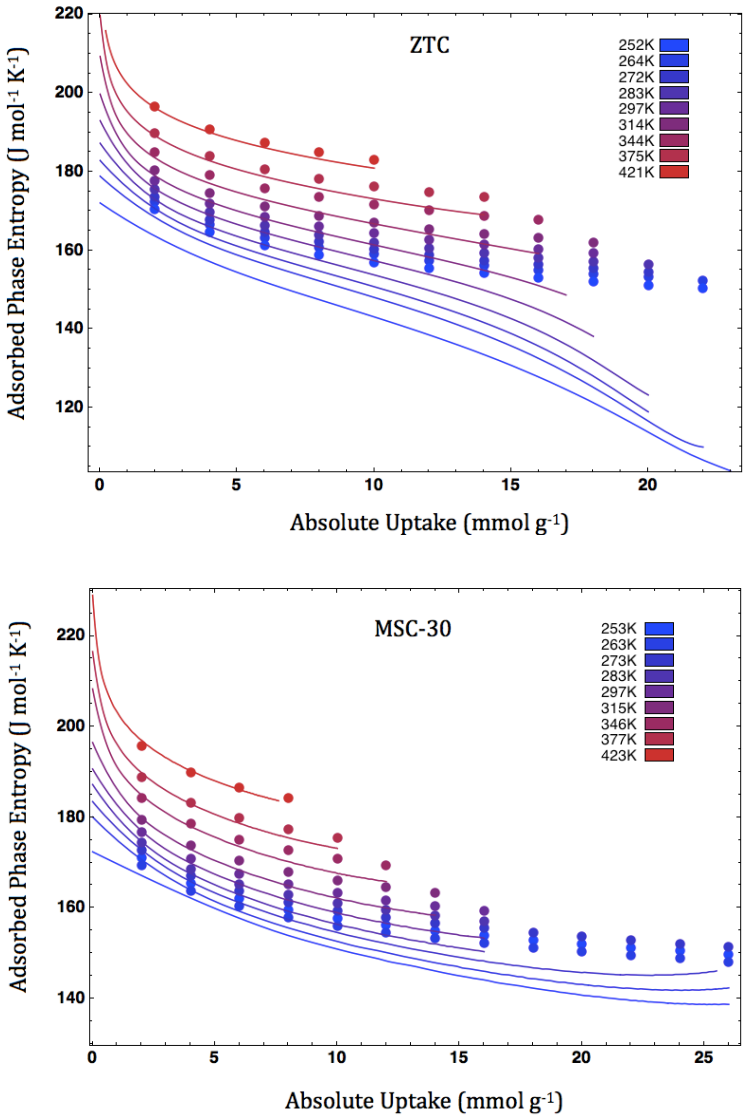

Figure 5. The molar adsorbed-phase entropies of ethane on ZTC and MSC-30. The curves indicate measured data and the points are calculated values (from statistical mechanics).

4.4 Statistical Mechanics

For comparison, the adsorbed-phase molar entropies were also calculated using statistical mechanics. Adsorbed ethane has numerous entropic contributions including vibrational, rotational, and configurational components. Each contribution was accounted for

as follows using standard partition functions and established values for characteristic frequencies. The effects of intermolecular interactions between the adsorbed molecules were not included, and the resulting discrepancies are discussed following the analysis.

Ethane in the gas phase has 12 internal vibrational modes with well-known characteristic vibrational frequencies and degeneracies,[30] and minimal changes in these frequencies are expected upon adsorption. Near ambient temperature, these vibrational modes are of little significance to the adsorbed-phase entropy, but their influence increases with temperature (see Figure 6). The partition function for vibrational modes ($q_{vib\,i}$) is:

$$q_{vib\,i}(T) = \frac{e^{-\Theta_{vib\,i}/2T}}{1-e^{-\Theta_{vib\,i}/T}} \qquad (9)$$

Here, $\Theta_{vib\,i}$ is the characteristic vibrational temperature of the i^{th} vibrational mode.

Adsorbed gases also vibrate with respect to the adsorbent surface. While the partition function for these vibrations is also given by Equation 9, the characteristic frequency is not readily accessible. Instead we have estimated these characteristic harmonic frequencies by

$$\nu = \left(\frac{1}{2\pi}\right)\sqrt{\frac{K}{m}} \qquad (10)$$

Here K is the force constant and m is the molecular mass (of ethane). For simplicity (in the absence of detailed knowledge of the adsorbent surface geometry) the adsorbate-adsorbent potential was modeled as a Lennard-Jones potential with ε given by the average Henry's law value of the isosteric heat per molecule. For a Lennard-Jones potential, the force constant and frequency are:

$$K = \frac{72\varepsilon}{{r_m}^2} \qquad (11)$$

$$\nu = \left(\frac{1}{2\pi}\right)\sqrt{\frac{72\varepsilon}{m(r_m)^2}} \quad (12)$$

Here r_m is the distance wherein the potential reaches its minimum. Rotationally, ethane is a symmetric top with characteristic frequencies $\Theta_{rota}=\Theta_{rotb}=0.953K$, $\Theta_{rotc}=3.85K$.[31] For ethane, the high temperature approximation of the partition function for the rotational modes (q_{rot}) is:

$$q_{rot} = \frac{\pi^{\frac{1}{2}}}{6}\left(\frac{T}{\Theta_{rota}}\right)\left(\frac{T}{\Theta_{rotc}}\right)^{\frac{1}{2}} \quad (13)$$

The configurational entropy of the adsorbed phase was determined using the partition function:

$$q_{con} = \left(\frac{\lambda}{\Lambda^2}\right)^{n_a} \quad (14)$$

Here λ is specific surface area divided by specific absolute uptake, and Λ is the thermal de Broglie wavelength. Using the partition functions above, individual entropy contributions were calculated by taking the negative temperature derivative of the Helmholtz free energy. These individual contributions were summed to obtain the total molar entropy of the adsorbed phase (shown in Figure 5). The relative contributions from each component to the total entropy at a representative fixed adsorption quantity are shown in Figure 6.

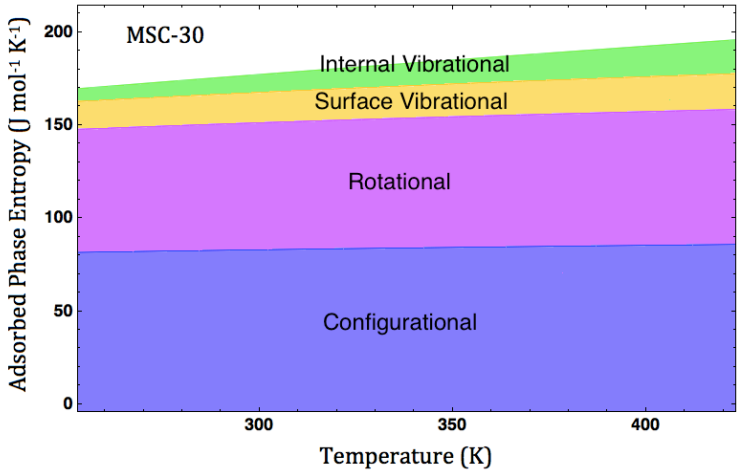

Figure 6. Relative contributions of each component to the total adsorbed-phase entropy of ethane on MSC-30 at the absolute uptake value of 2 mmol g^{-1}.

As shown in Figure 5, there is good agreement between the measured and calculated values of the adsorbed-phase entropy of ethane on MSC-30. Errors are less than 10% (without applying any fitting or offset) throughout the measured regime, and are especially low at high temperatures. At high coverages the measured entropy of ethane on MSC-30 gradually levels out, but maintains positive concavity. In contrast, the measured entropy of ethane adsorbed on ZTC deviates significantly from calculated values. At high temperatures, the measured entropy is in agreement with the calculation from statistical mechanics, as in MSC-30. However, at low temperatures and high coverages, the measured entropy is well below the calculated value (with discrepancies of up to 42%). This is associated with the increase in isosteric heat in this regime; ethane adsorption on ZTC has an anomalously increasing isosteric heat, and likewise an anomalously decreasing entropy in the adsorbed phase. This is expected to be caused by enhanced adsorbate-absorbate interactions on the surface of ZTC. Stronger intermolecular interactions correspond to stiffer vibrational modes, hindered rotational motion, and inhibited

molecular motion/rearrangement, all of which can lead to a decrease in the entropy of the adsorbed phase.

The increase in isosteric heat above the Henry's Law value is largest at low temperatures. We expect that temperature will disrupt the adsorbate-adsorbate lateral interactions, suppressing the increase in isosteric heat. The thermal behavior may be a cooperative one, where the loss of lateral interactions makes other lateral interactions less favorable. There appears to be a critical temperature around 300 K where the effect of lateral interactions between ethane molecules is lost.

5. Conclusions

Ethane adsorption was measured on a zeolite-templated carbon material (ZTC) that has an exceptionally high surface area and narrow and uniform microporosity. An increasing isosteric heat of adsorption as a function of coverage was observed. The isosteric heat rises by 4.6 kJ mol^{-1} from a Henry's law value of 20.6 kJ mol^{-1} at low coverage to a peak of 25.2 kJ mol^{-1} at a coverage of 21.4 mmol g^{-1}. By comparing ethane adsorption on ZTC to methane adsorption on the same material, it was found that the slope of the isosteric heat of adsorption with coverage approximately scales with the strength of the adsorbate-adsorbate intermolecular interactions. A control material, superactivated carbon MSC-30, behaved as a normal microporous carbon adsorbent, exhibiting a monotonically decreasing isosteric heat with coverage. The measured adsorbed-phase entropy of ethane on MSC-30 was also successfully estimated with a statistical mechanics based approach (without intermolecular interactions), exhibiting discrepancies of less than 10%. The measured entropy of ethane adsorbed on ZTC deviated significantly from this standard model prediction at high coverage

and low temperature, indicating atypical adsorption properties in this system. The behavior of both the adsorbed-phase entropy and the isosteric heat of ethane on ZTC can be explained by attractive adsorbate-adsorbate interactions promoted by the nanostructured surface of ZTC.

References:

1. Magnowski, N. B. K.; Avila, A. M.; Lin, C. C. H.; Shi, M.; Kuznicki, S. M. Extraction of Ethane from Natural Gas by Adsorption on Modified ETS-10. *Chem. Eng. Sci.* **2011**, *66*, 1697-1701.
2. Sircar, S. Pressure Swing Adsorption. *Ind. Eng. Chem. Res.* **2002**, *41*, 1389-1392.
3. Sircar, S. Basic Research Needs for Design of Adsorptive Gas Separation Processes. *Ind. Eng. Chem. Res.* **2006**, *45*, 5435-5448.
4. Tan, Z.; Gubbins, K. E. Selective Adsorption of Simple Mixtures in Slit Pores - A Model of Methane Ethane Mixtures in Carbon. *J. Phys. Chem.* **1992**, *96*, 845-854.
5. Jiang, S. Y.; Zollweg, J. A.; Gubbins, K. E. High-Pressure Adsorption of Methane and Ethane in Activated Carbon and Carbon-Fibers. *J. Phys. Chem.* **1994**, *98*, 5709-5713.
6. Amora, M. R., Jr.; Canabrava, D. V.; Bastos-Neto, M.; Torres, A. E. B.; Cavalcante, C. L., Jr.; Azevedo, D. C. S. Equilibrium Adsorption of Binary Mixtures of Light Hydrocarbons in Activated Carbon. *Lat. Am. Appl. Res.* **2009**, *39*, 153-156.
7. Xia, Y.; Walker, G. S.; Grant, D. M.; Mokaya, R. Hydrogen Storage in High Surface Area Carbons: Experimental Demonstration of the Effects of Nitrogen Doping. *J. Am. Chem. Soc.* **2009**, *131*, 16493-16499.
8. Goj, A.; Sholl, D. S.; Akten, E. D.; Kohen, D. Atomistic Simulations of CO2 and N-2 Adsorption in Silica Zeolites: The Impact of Pore Size and Shape. *J. Phys. Chem. B* **2002**, *106*, 8367-8375.
9. Coasne, B.; Pellenq, R. J. M. Grand Canonical Monte Carlo Simulation of Argon Adsorption at the Surface of Silica Nanopores: Effect of Pore Size, Pore Morphology, and Surface Roughness. *J. Chem. Phys.* **2004**, *120*, 2913-2922.
10. Lozano-Castello, D.; Cazorla-Amoros, D.; Linares-Solano, A.; Quinn, D. F. Influence of Pore Size Distribution on Methane Storage at Relatively Low Pressure: Preparation of Activated Carbon with Optimum Pore Size. *Carbon* **2002**, *40*, 989-1002.
11. Alcaniz-Monge, J.; Lozano-Castello, D.; Cazorla-Amoros, D.; Linares-Solano, A. Fundamentals of Methane Adsorption in Microporous Carbons. *Micropor. Mesopor. Mat.* **2009**, *124*, 110-116.
12. Panella, B.; Hirscher, M.; Roth, S. Hydrogen Adsorption in Different Carbon Nanostructures. *Carbon* **2005**, *43*, 2209-2214.
13. Poirier, E.; Chahine, R.; Bose, T. K. Hydrogen Adsorption in Carbon Nanostructures. *Int. J. Hydrogen Energ.* **2001**, *26*, 831-835.
14. Bhatia, S. K.; Myers, A. L. Optimum Conditions for Adsorptive Storage. *Langmuir* **2006**, *22*, 1688-1700.
15. Mason, J. A.; Veenstra, M.; Long, J. R. Evaluating Metal-Organic Frameworks for Natural Gas Storage. *Chem. Sci.* **2014**, *5*, 32-51.
16. Stadie, N. P.; Murialdo, M.; Ahn, C. C.; Fultz, B. Anomalous Isosteric Enthalpy of Adsorption of Methane on Zeolite-Templated Carbon. *J. Am. Chem. Soc.* **2013**, *135*, 990-993.

17. Yuan, B.; Wu, X.; Chen, Y.; Huang, J.; Luo, H.; Deng, S. Adsorptive Separation Studies of Ethane-Methane and Methane-Nitrogen Systems Using Mesoporous Carbon. *J. Colloid Interface Sci.* **2013**, *394*, 445-450.
18. Nishihara, H.; Hou, P.-X.; Li, L.-X.; Ito, M.; Uchiyama, M.; Kaburagi, T.; Ikura, A.; Katamura, J.; Kawarada, T.; Mizuuchi, K.; Kyotani, T. High-Pressure Hydrogen Storage in Zeolite-Templated Carbon. *J. Phys. Chem. C* **2009**, *113*, 3189-3196.
19. Dubinin, M. M.; Radushkevich, L. V. Equation of the Characteristic Curve of Activated Charcoal. *Proc. Acad. Sci. USSR Phys. Chem. Sect.* **1947**, 55, 331-337.
20. Nguyen, C.; Do, D. D. The Dubinin-Radushkevich Equation and the Underlying Microscopic Adsorption Description. *Carbon* **2001**, *39*, 1327-1336.
21. Brunauer, S.; Emmett, P. H.; Teller, E. Adsorption of Gases in Multimolecular Layers. *J. Am. Chem. Soc.* **1938**, *60*, 309-319.
22. Tarazona, P.; Marconi, U. M. B.; Evans, R. Phase-Equilibria of Fluid Interfaces and Confined Fluids - Nonlocal Versus Local Density Functionals. *Mol. Phys.* **1987**, *60*, 573-595.
23. Dumas, J. B. A Method of Estimating Nitrogen in Organic Material. *Ann. Chim. Phys.* **1833**, 58, 171-173.
24. Stadie, N. P.; Vajo, J. J.; Cumberland, R. W.; Wilson, A. A.; Ahn, C. C.; Fultz, B. Zeolite-Templated Carbon Materials for High-Pressure Hydrogen Storage. *Langmuir* **2012,** *28*, 10057-10063.
25. Bowman, R. C.; Luo, C. H.; Ahn, C. C.; Witham, C. K.; Fultz, B. The Effect of Tin on the Degradation of LANI5-YSNY Metal-Hydrides During Thermal Cycling. *J. Alloys Compd.* **1995**, *217*, 185-192.
26. Lemmon, E. W.; Huber, M. L.; McLinden, M. O. *NIST Standard Reference Database 23: Reference Fluid Thermodynamic and Transport Properties-REFPROP*, Version 8.0 [CD-ROM], 2007.
27. Mertens, F. O. Determination of Absolute Adsorption in Highly Ordered Porous Media. *Surf. Sci.* **2009**, *603*, 1979-1984.
28. Sircar, S. Gibbsian Surface Excess for Gas Adsorption - Revisited. *Ind. Eng. Chem. Res.* **1999**, *38*, 3670-3682.
29. Tee, L. S.; Gotoh, S.; Stewart, W. E. Molecular Parameters for Normal Fluids - Lennard-Jones 12-6 Potential. *Ind. Eng. Chem. Fundam.* **1966**, *5*, 356-363.
30. Shimanouchi, T. Tables of Molecular Vibrational Frequencies Consolidated Volume 2. *J. Phys. Chem. Ref. Data* **1977**, *6*, 993-1102.
31. Chao, J.; Wilhoit, R. C.; Zwolinski, B. J. Ideal Gas Thermodynamic Properties of Ethane and Propane. *J. Phys. Chem. Ref. Data* **1973**, 2, 427-437.